UNIVERSITY OF ICELAND

FACULTY OF CIVIL AND ENVIRONMENTAL ENGINEERING
VR-II – Hjardarhagi 2-6, 107 Reykjavik, Iceland
Tel. +354 525 4700 · von.hi.is

Manuscript published in 'Geotechnical Testing Journal'

Elin Asta Olafsdottir, Bjarni Bessason, Sigurdur Erlingsson, Amir M. Kaynia. (2024). A Tool for Processing and Inversion of MASW Data and a Study of Inter-session Variability of MASW. *Geotechnical Testing Journal*, 47(5), 1006–1025. https://doi.org/10.1520/GTJ20230380

Date of acceptance:
February 01 2024

Title:
A Tool for Processing and Inversion of MASW Data and a Study of Inter-Session Variability of MASW

Authors:
Elin Asta Olafsdottir
Faculty of Civil and Environmental Engineering, University of Iceland, Reykjavik, Iceland
E-mail: elinasta@hi.is

Bjarni Bessason
Faculty of Civil and Environmental Engineering, University of Iceland, Reykjavik, Iceland
E-mail: bb@hi.is

Sigurdur Erlingsson
Pavement Technology, Swedish National Road and Transport Research Institute (VTI), Linköping, Sweden
Faculty of Civil and Environmental Engineering, University of Iceland, Reykjavik, Iceland
E-mail: sigurdur.erlingsson@vti.se

Amir M. Kaynia
Department of Structural Engineering, Faculty of Engineering, Norwegian University of Science and Technology, Trondheim, Norway
Norconsult AS, Sandvika, Norway
Email: amir.kaynia@ntnu.no

Corresponding author:
Sigurdur Erlingsson
Pavement Technology, Swedish National Road and Transport Research Institute (VTI), Linköping, Sweden
Faculty of Civil and Environmental Engineering, University of Iceland, Reykjavik, Iceland
E-mail: sigurdur.erlingsson@vti.se

A Tool for Processing and Inversion of MASW Data and a Study of Inter-Session Variability of MASW

Elin Asta Olafsdottir[1], Bjarni Bessason[1], Sigurdur Erlingsson[1,2], and Amir M. Kaynia[3,4]

[1]Faculty of Civil and Environmental Engineering, University of Iceland, Reykjavik, Iceland

[2]Pavement Technology, Swedish National Road and Transport Research Institute (VTI), Linköping, Sweden

[3]Department of Structural Engineering, Faculty of Engineering, Norwegian University of Science and Technology, Trondheim, Norway

[4]Norconsult AS, Sandvika, Norway

Abstract

Multichannel Analysis of Surface Waves (MASW) is a non-invasive active-source technique for determination of near-surface shear wave velocity (V_S) profiles. Here we introduce and describe MASWavesPy, an open-source Python package for processing and inverting MASW data, whose design follows an object-oriented paradigm. To assess the performance of the new tool, measurements were conducted at four benchmark sites in Norway, characterized as silt, soft clay, silty sand, and quick clay. The results show that the V_S profiles obtained with MASWavesPy compare well with those obtained previously at the respective sites using invasive, non-invasive and laboratory techniques. Furthermore, the efficiency and usability of the new package is superior to previous versions developed by same authors. The software can

be accessed through the Python Package Index (PyPI) at https://pypi.org/project/maswavespy/ , along with sample data. This work further explores the inter-session variability of MASW measurements for civil engineering applications at soft soil sites. For this purpose, repeated measurements were conducted over a seven-year period at a silty sand site in South Iceland and the recorded time series analysed using the newly developed tool. The inter-session variability of the analysis results is reported in terms of Rayleigh wave phase velocity, interval V_S profiles, and time-averaged V_S for reference depths commonly used in practise.

Keywords

Multichannel Analysis of Surface Waves (MASW), shear wave velocity, open-source software, benchmarking, inter-session variability

Introduction

Shear wave velocity (V_S) is a key parameter for evaluating the dynamic response of soil, including predictions of seismic site response, analysis of vibration transmissions and soil-structure interaction. The time-averaged V_S in the top-most 30 m ($V_{S,30}$), or down to a reference depth H ($V_{S,H}$), is also commonly used as a proxy to classify soil sites based on expected soil amplifications for, e.g., ground motion predictions (Douglas and Edwards 2016) and simplified assessments of seismic site response in design codes (CEN 2004; BSSC 2020). Moreover, it has been shown that in dynamic soil-structure interaction problems, it is the average V_S across the interaction domain that governs the response rather than pointwise soil characteristics as determined by, e.g., CPT soundings (Kaynia 2021).

Surface wave methods (SWMs) are non-invasive geophysical techniques that use the dispersive properties of surface waves, commonly Rayleigh waves, for evaluation of V_S. Compared to invasive measurements, SWMs are both time- and cost-efficient. SWMs can be used for a wide variety of ground conditions, including very dense or coarse-grained sediments, cemented soils and mixed soils containing cobbles and boulders. The results obtained with SWMs will indicate an average of the soil stiffness parameters over the tested area. This is important from a design perspective, as it mitigates the effect of the inherent variability associated with pointwise data (Kaynia 2021). However, the resolution of SWMs decreases with depth and the inverse problem encountered in the data analysis is inherently non-unique. Hence, given the experimental uncertainties, multiple velocity models may be viewed as equivalent solutions. If both invasive and non-invasive measurements of V_S are available for a particular site, the invasive measurements are typically regarded as benchmark values. Several such studies have been conducted to evaluate the performance of different SWMs (e.g., Boore and Asten 2008; Garofalo et al. 2016b). Intra-method comparative studies also exist where multiple teams have

58 analysed a common seismic dataset (Tran and Hiltunen 2011; Cox, Wood, and Teague 2014;
59 Garofalo et al. 2016a). Studies on the direct repeatability of both the data acquisition and
60 analysis are less common but have been conducted by repeated active-source measurements in
61 close proximity in a particular session (Donohue and Long 2008) or over a few months period
62 (Beaty and Schmitt 2003). Endrun, Ohrnberger, and Savvaidis (2010) further analysed the
63 temporal consistency of dispersion and spatial autocorrelation curves retrieved over a span of
64 several years. However, their study was aimed at ambient vibration measurements only.

65 In recent years, the linear data acquisition layout of the MASW method (Multichannel Analysis
66 of Surface Waves) (Park, Miller, and Xia 1999a) has become widespread in civil engineering
67 practice to retrieve the V_S distribution down to 20–30 m depth (Foti et al. 2018). A number of
68 software solutions exist to process MASW data, both open-source tools (e.g., Wathelet,
69 Jongmans, and Ohrnberger 2004; Wathelet et al. 2020; Teague, Wood, and Cox 2017;
70 Vantassel 2021; Vantassel and Cox 2022) and commercial software. The authors of this study
71 have previously developed a basic open-source MATLAB computational package,
72 MASWaves (http://masw.hi.is), for acquiring and interpreting MASW data (Olafsdottir 2019;
73 Olafsdottir, Erlingsson, and Bessason 2018a, 2020; Olafsdottir et al. 2019). The main
74 incentives for developing the software from scratch were to gain easy access and flexibility to
75 modify and adapt the processing and analysis tools for further developments and engineering
76 applications. This work has laid the foundations for a new adaptive object-oriented Python
77 package, MASWavesPy, for processing and analysing multi-channel surface wave
78 registrations. The new package includes a set of additional tools and technical advancements
79 to both the dispersion processing and inversion analysis schemes, aimed at improving the
80 efficiency, usability, and performance of the code. The phase shift method (Park, Miller, and
81 Xia 1998) is implemented to transform recorded time series into the frequency-phase velocity
82 domain, and a specially designed GUI application is included to aid identification and

extraction of experimental dispersion curves. The package further includes modules to combine dispersion curves retrieved from multiple shot gathers and to assess experimental uncertainties. The inversion module is based on an efficient Monte Carlo global-search, with the fast delta-matrix algorithm (Buchen and Ben-Hador 1996) used for forward computations. Computationally intensive parts of the analysis and inversion tools are written in Cython (C extension for Python) (Behnel et al. 2010) for improved code performance and computational speed. Hence the new package provides highly improved computational time as compared to the original MASWaves formulation.

This study aims to explore the long-term inter-session variability of MASW measurements for civil engineering site characterization. For this purpose, repeated measurements were conducted over a seven-year period at a silty sand site in South Iceland. The processing and inversion of the recorded time series was conducted using the new MASWavesPy package. To validate the tool's performance, measurements were conducted at four benchmark sites in Norway (Lunne, Long, and Forsberg 2003; L'Heureux et al. 2017) that are characterized by commonly encountered types of soft soils. The resulting velocity profiles were compared to in-situ and laboratory measurements of V_S conducted by different teams of researchers.

Method

Application of MASW can be divided into three steps: data acquisition (DAQ), processing and inversion. For data acquisition, low-frequency receivers are lined up with equal spacing on the surface and an impact load is applied in-line with the receiver array at a certain offset from the first (or last) receiver. The hardware used in this study consisted of a pair of NI USB-6218 multifunction I/O devices from National Instruments and a set of GS-11D 4.5 Hz vertical geophones from Geospace Technologies.

The data processing is aimed at identifying the dispersion characteristics of the acquired Rayleigh waves over a range of frequencies. This is achieved with spectral processing that visualizes the energy density of the multi-channel time series and allows for identification of modal dispersion curve(s) based on the observed spectral maxima. Here, the focus is on evaluation and inversion of the fundamental mode dispersion curve. Therefore, in the following, the term 'dispersion curve' (DC) will refer to its fundamental mode. Previous studies have found MASW type data acquisition and analysis well suited for identifying higher mode DC components (e.g., Gabriels, Snieder, and Nolet 1987; Park, Miller, Xia 1999b; Vantassel et al. 2022). If the aim is to invert multiple modes simultaneously, the code can be easily configured to include higher modes in the analysis. However, our experience shows that analysis using the fundamental mode yields sufficient results for commonly encountered stratigraphic conditions. If excited, higher modes may add to the uncertainty of the model parameter estimation due to the risk of mode misidentification in cases where the spectral resolution of the dispersion image is insufficient. It should be noted that consideration of higher modes may be necessary at sites with complex stratigraphy (e.g., the presence of strong velocity contrasts or reversals). Such conditions are, however, outside the scope of the current study.

The optimal configuration of the MASW receiver array (e.g., array length, geophone spacing, and source-receiver offsets) depends on the intended survey depth, the available equipment, and the velocity structure of the tested site. A summary of typical DAQ parameters is, e.g., provided by Foti et al. (2018). The seismic datasets used in this work include a statistical sample of DCs, obtained by different receiver array configurations and source-receiver offsets (arrays with a common midpoint) and by collecting repeated shots for a given configuration, as recommended in prior studies (Cox and Wood 2011; Bessason and Erlingsson 2011). The different array set-ups provide information on different volumes of soil and can help detect significant lateral variations in soil properties beneath the array. Comparison of DCs retrieved

using multiple source offsets also aids identification of potential near-field effects in the acquired data (Wood and Cox 2012), which result in an irregular and unreliable amplitude trend in the dispersion image at low frequencies. The variability in the retrieved phase velocity values with frequency (or wavelength) is thus an indicator of the data reliability (Foti et al. 2018) and of value for, e.g., selection of representative V_S models and assessment of inversion uncertainties. A simple empirical criterion to reduce DC errors due to near-field effects to below 10–15 % was proposed by Yoon and Rix (2009), restricting the maximum DC wavelength (λ_{max}) by the array centre distance ($\overline{x}$) as $\overline{x}/\lambda_{max} \geq 1$. It has, however, been found overly restrictive in some cases (Wood and Cox 2012; Li and Rosenblad 2011). Hence, if experimental DCs are identified from shots collected with a variety of source offsets, a recent study has suggested that the near-field criterion may be relaxed for some of the shorter-offset shots, given that the low-frequency part of the corresponding DCs is verified by comparison with one that meets the criterion (Rahimi, Wood, and Himel 2022). The prospective depth of the resulting interval V_S profiles (z_{max}) is strongly affected by the range of retrieved wavelengths (λ_{min} to λ_{max}). For inversion of fundamental mode DCs, common practice (e.g., Park, Miller, and Xia 1999a; Foti et al. 2018) is to limit the maximum depth to $\lambda_{max}/3$ to $\lambda_{max}/2$ and the thickness of the surficial layer to $\lambda_{min}/3$ to $\lambda_{min}/2$. This approach is subsequently referred to as the λ-criterion. Thus, if combined with the guidelines of Rahimi, Wood, and Himel (2022), z_{max} becomes directly related to the longest array centre distance(s) adopted during DAQ.

The inversion assumes that the surveyed site can be modelled as a layered elastic medium consisting of n finite-thickness, homogeneous and isotropic layers over a half-space. Each layer is described by its shear wave velocity, compressional wave velocity (V_P) (or Poisson's ratio, ν), mass density (ρ) and thickness (h). Hence, the inversion step entails solving a model parameter identification problem using the experimental DC as a target. At frequencies above

5 Hz, V_S and h have a dominant effect on the fundamental mode DC (Xia, Miller, and Park 1999). As the effect of change in V_P (or ν) and ρ is less significant, these parameters are fixed based on a-priori information or by using standard values, thus, reducing the number of inversion parameters. The groundwater level is specified based on in-situ observations and available data. The parameterization of the surveyed site is further an important consideration during the inversion process. A stratified model consisting of too few layers may produce an oversimplified depiction of the true variation in V_S with depth. However, including too many layers may also result in inaccurate interval velocity profiles, because of the inversion being severely over-determined. Hence, the number of layers is regarded as an additional inversion parameter and a preliminary analysis conducted using different values of n. This approach is consistent with recommendations in the literature (Cox and Teague 2016; Foti et al. 2018).

MASWavesPy Approach

Figure 1 provides a graphical overview of the workflow of MASWavesPy. The package consists of four primary data processing modules; `wavefield`, `dispersion`, `combination`, and `inversion`, and two supplementary modules; `dataset` and `select_dc`.

The function of the `wavefield` module is to import and view the acquired multi-channel time series, with each imported record being contained in a separate `RecordMC` object. The recorded data should be provided as text files, or as waveform files compatible with the `obspy.read()` function from the ObsPy library (Beyreuther et al. 2010; Krischer et al. 2015), e.g., SEG-2 formatted files. The `dispersion` module provides methods for dispersion processing of the imported data. Each recorded wavefield is transformed into the frequency-phase velocity domain (Park, Miller, and Xia 1998) and is used to initialize an `ElementDC` object, which contains methods for visualization of the phase velocity spectrum and DC

extraction. A DC obtained from a single multi-channel registration (i.e., a single instance of `RecordMC`) is hereafter referred to as an 'elementary dispersion curve' and stored in a single instance of `ElementDC`. Elementary DCs are identified based on observed spectral maxima by a GUI application provided in the supplementary `select_dc` module.

The purpose of the third data processing module (`combination`) is to combine elementary DCs obtained from multiple surface wave registrations (i.e., associated with multiple `ElementDC` objects). A `CombineDCs` object contains the composite DC and provides methods to assess and visualize the spread in the dispersion data, both in the frequency-phase velocity and phase velocity-wavelength domains. It is encouraged to visually inspect the set of identified elementary DCs in the frequency-phase velocity domain to identify potentially biased DCs (e.g., due to near-field effects, higher-mode interference, or imprecise DC picking), and to assess if the degree of variability of the DC data points with frequency is reasonable given observed trends at other sites (e.g., Passeri et al. 2021). The composite DC, here specified as an inversion target, is subsequently obtained by grouping the elementary dispersion curve data points within $\log_a$ spaced wavelength bands, with the parameter a being specified on a per-dataset basis (Bessason and Erlingsson 2011; Olafsdottir, Bessason, and Erlingsson 2018b). The arithmetic mean of the phase velocity values within each interval is used as a point estimate of the phase velocity of the Rayleigh wave components in the given wavelength range. Their standard deviation represents the spread of the dispersion curve data points within each wavelength band and is implemented in the post-processing of the sampled V_S profiles as described below. Practical recommendations on the wavelength-binning and associated parameter selection are provided in Olafsdottir, Bessason, and Erlingsson (2018b). In particular, the width of the wavelength intervals should be specified such that bins showing abnormally small standard deviations, resulting from, e.g., a clustered distribution of the elementary DC data points or only a handful of data points belonging to certain bins, are

avoided. In such cases, the calculated standard deviation may not be representative of the true variability of the phase velocity values and can, in later steps of the analysis, bias the selection criteria for 'accepted' V_S profiles. The supplementary `dataset` module is used to import and manage seismic datasets, consisting of numerous multi-channel records, through `Dataset` objects. A `Dataset` object can contain multiple `RecordMC` and associated `ElementDC` objects and provides routines for initializing a `CombineDCs` for the set of acquired records or a particular subset of records.

The `inversion` module is used to evaluate the V_S profile of the surveyed site by inverting the composite DC (or a particular elementary DC). The inversion routines are defined on an `InvertDC` object, which is initialized using a given experimental DC. The initial layering parameterization (i.e., the number of layers and associated layer thicknesses) is required as a starting point for the inversion process, along with an initial estimate of V_S for each layer. If additional geotechnical data is available for the tested site, including boring logs or soundings (e.g., CPT, SPT or DMT), it is advised to use this data to guide the initial parameter assessments regarding number of layers, expected locations of layer interfaces and credible starting values for V_S given the encountered soil types. If the initial parameters must be assessed without a priori information on the site conditions, preliminary analysis using several different parameterizations and starting values, as has been strongly encouraged in literature (e.g., Cox and Teague 2016; Foti et al. 2018), is recommended. The inversion is conducted using an efficient Monte Carlo global-search (Olafsdottir, Erlingsson, and Bessason 2020) and the fast delta-matrix algorithm (Buchen and Ben-Hador 1996) for forward computations. The shear wave velocity and layer thicknesses are specified as inversion parameters. The misfit (ϵ_{DC}) between the target experimental and theoretical DCs is here computed as,

$$\epsilon_{DC} = \frac{1}{Q}\sum_{q=1}^{Q} \frac{\sqrt{\left(V_{R,t,q} - V_{R,e,q}\right)^2}}{V_{R,e,q}} \cdot 100\ \% \qquad (1)$$

where $V_{R,t}$ and $V_{R,e}$ denote the theoretical and experimental phase velocities, respectively. Hence, when inverting DCs with defined upper and lower boundaries, the boundary DCs are, for the sake of simplicity, not included in the misfit calculations. However, if it is deemed beneficial for individual use cases, the definition of the misfit function can easily be altered within the MASWavesPy code, e.g., to introduce a function that weighs the differences between the experimental and theoretical values by the calculated uncertainty.

Several post-processing routines are defined on the `InvertDC` objects to help draw inference from the set of sampled V_S models. 'Accepted' interval V_S profiles are here defined as the set of profiles whose associated theoretical DCs fall between the experimental DC boundaries, specified as m standard deviations of the average curve, at all wavelengths. Wavelength-binning of the elementary DCs is preferred for this purpose to ensure an equal value of λ_{max} for the average and boundary curves. Values of m = 1, m = 1.5, or m = 2 standard deviations have been found to perform well for sites with a similar soil stratigraphy and a comparable degree of DC variation as those presented in this work. For applications discussed in later sections, m is specified as 1. If the standard deviation of the composite DC is much lower at certain wavelengths than for the remainder of the curve, that would in turn dominate the selection of 'accepted' profiles as described above, it may be better to use a different procedure to define a set of 'accepted' profiles. Other approaches, commonly encountered in surface wave inversion, include implementing a misfit criterion or presenting a given number of 'best fitting' profiles. Selecting or sampling a fixed number of V_S models showing sufficiently low misfit values may, however, underrepresent the true variability in the experimental data. A recent study has introduced an alternative procedure for improved quantification of V_S uncertainty, particularly focusing on propagating the experimental data variability into the resulting set of 'accepted' V_S profiles (Vantassel and Cox 2021).

The set of accepted profiles can subsequently be summarized in terms of its median or mean profiles. In addition, sampled (or inferred) interval velocity profiles can be presented as $V_{S,z}$,

$$V_{S,z} = \frac{z}{tt(z)} \quad (2)$$

$tt(z)$ is the travel time of shear waves from the surface to depth z obtained as,

$$tt(z) = \sum_{i=1}^{N} \left(\frac{h_i}{V_{S,i}}\right) \quad (3)$$

where $V_{S,i}$ and h_i denote the shear wave velocity and thickness of the i-th layer, respectively, for a total of N layers down to depth z. For assessment of $V_{S,z}$ for $z > d$, where d is the depth of the half-space top, the interval velocity profiles are extrapolated using the half-space velocity. This approach is consistent with the simplest method of Boore (2004) for estimation of $V_{S,30}$ from shallow models,

$$V_{S,30} = \frac{30}{tt(d) + \frac{30-d}{V_{eff}}} \quad (4)$$

where V_{eff} equals the half-space V_S. It is also in line with the recommendations in BSSC (2020) for sites where V_S has been measured down to 15–30 m and soft (low velocity) layers are not expected beneath that depth.

Repeatability of the MASW Analysis

Repeated MASW measurements were conducted between 2013 and 2019 at Arnarbæli in South Iceland. The test site is located on the western bank of the Ölfus River, between the towns of Hveragerði and Selfoss, and less than 2 km from the western fault rupture of the M_w6.3 May 2008 Ölfus earthquake (fig. 2). The site is characterized by thick sediments of Holocene glaciofluvial silty sand. Two test pits were dug at the site in September 2022 to assess the

groundwater level under typical conditions. The water level in both pits was 10–20 cm below surface.

Data Acquisition and Processing, Intra-Session Variability

Six separate MASW datasets were collected in September 2013 (M-13), August 2014 (M-14), July 2015 (M-15), September 2017 (M-17), May 2018 (M-18), and June 2019 (M-19). An array of 24 geophones was used for the data acquisition, except in the 2017-session, where an array of 16 geophones was used. The impact load was created with a 6.3 kg sledgehammer, with vertical strikes applied either on a 15 cm-diameter metallic plate or directly on the ground surface. The sampling rate was 1000 Hz and the recording time either 1.2 or 2.2 s, including a 0.2 s pre-trigger. The midpoints of the six survey profiles (M-13 to M-19) were positioned within a 2 m radius and their orientation was the same in a southeast to northwest direction. Table 1 summarizes the array-source configurations used in each DAQ session, i.e., the geophone spacing(s) and the range of source offsets. Repeated shots (usually four to six) were collected at each offset. The multi-channel records acquired with a given configuration were left unstacked and each record processed separately to retrieve an estimate of the site's DC.

Table 1 *Overview of MASW datasets at Arnarbæli site*

		M-13	**M-14**	**M-15**	**M-17**	**M-18**	**M-19**
Data acquisition							
Month and year		September 2013	August 2014	July 2015	September 2017	May 2018	June 2019
No. geophones	[-]	24	24	24	16	24	24
Geophone spacing (source offsets)	[m]	1 (3–20)	0.5 (5–10) 1 (10–30) 2 (10–30)	0.5 (3–10) 1 (5–30) 2 (5–30)	2 (5–25)	0.5 (3–10) 1 (5–30) 2 (5–30)	0.5 (3–10) 1 (5–20) 2 (5–30)
No. records	[-]	32	55	96	21	65	88
Dispersion analysis							
DC frequency range	[Hz]	7.5–28.3	6.7–30.0	5.5–37.3	6.2–30.5	6.4–34.1	5.5–42.7
COV_{V_R} range	[%]	1.6–5.3	0.7–5.7	0.9–8.0	0.5–9.2	1.6–5.8	0.6–5.9

Figures 3*A–F* (top panels) show typical dispersion images of records acquired in each session. The spectra shown for sessions M-13, M-14, M-15, M-18, and M-19 were obtained with a 23 m receiver array (24 geophones spaced at 1 m intervals). For session M-17, the array length was 30 m (16 geophones spaced at 2 m intervals). The elementary DCs that were identified from the repeated shots (and the different array-source configurations) are shown in the middle panels of figures 3*A–F*, where they are categorised by receiver array length. For mitigation of near-field effects, λ_{max} of the composite DC for each session was limited by the respective maximum array centre distance. The elementary DCs obtained with the different array-source configurations were compared to identify those that showed potential signs of near-field effects, including abnormally low phase velocity values at low frequencies, apparent oscillations or roll-off. Those parts of the elementary DCs were excluded before further analysis and inversion. This approach is in line with the recommendations of Rahimi, Wood, and Himel (2022) in cases where the multiple source offset approach is used. It should be noted that in many cases where the array-source configuration clearly violated the near-field criteria of Yoon and Rix (2009) (i.e., $\overline{x}/\lambda < 1$), no obvious signs of near-field effects were seen in the resulting elementary DCs, as compared to those fulfilling the criteria. This is, e.g., consistent with previous observations reported by Wood and Cox (2012). The intra-session variability of the picked phase velocity values is quantified by the coefficient of variation (equation (5)) and shown in the bottom panels of figures 3*A–F*. $\overline{V_R}$ denotes the average phase velocity at a given frequency and s is the corresponding standard deviation.

$$COV_{V_R} = \frac{s}{\overline{V_R}} \tag{5}$$

The identified elementary DCs were consistent as indicated by an average intra-session COV_{V_R} of 2.5–3.3 %, with the lower frequency components displaying more variation than those of higher frequencies. Analysis of shots applied at different ends of the receiver array (forward

315 and reverse, fig. 3*A*), further indicated nearly identical DCs, therefore not implying significant
316 lateral variations in soil properties or stratigraphy beneath the array.

317 **Inter-Session Variability**

318 The elementary DCs from each session (figs. 3*A–F*, middle panels) were combined within
319 logarithmically-spaced wavelength bands. The resulting composite DCs (mean ± one standard
320 deviation) are shown in figure 3*G*. The variability in the population of mean DCs is quantified
321 in terms of COV_{V_R} (equation (5)) in figure 3*H* and can be seen as an indicator of the inter-
322 session variability in the experimental dispersion data. The computed COV_{V_R} values are below
323 5 %, except in the shortest wavelength range (< 3.5 m) where they increase rapidly with
324 decreasing wavelength. However, the sample size used to compute the COV-statistic is very
325 small (fig. 3*I*). Its values should, therefore, be interpreted with caution. Nevertheless, it is used
326 for consistency with the evaluation of the intra-session variability and to allow for comparison
327 with studies in the literature.

328 Several different parameterizations, consisting of three to eight layers (where the bottom layer
329 is a half-space), were tested to assess the effects of the model parameterization on the inverted
330 V_S profiles. As the backcalculation process includes a Monte Carlo-based optimization, the
331 inversion scheme was initiated 25 times (for each parameterization) to reduce the effects of the
332 randomized sampling on the inversion results. 1,000 trial V_S profiles were sampled in each
333 initiation. Inference was subsequently drawn from the resulting sets of 25×1,000 trial profiles.
334 As the groundwater table at the site is very close to surface, all layers were modelled as
335 saturated. The mass density profile was specified using existing laboratory-measured values
336 (Green et al. 2012) and the V_P of the saturated soil was specified as 1,500 m/s. Apart from the
337 three-layer parameterization, the resulting interval V_S profiles all presented a similar trend and
338 provided comparable misfit values. However, smoother interval velocity profiles, that are

considered to better represent the true site conditions, were obtained by a parameterization including at least five to seven layers. A six-layer model was therefore selected for assessment of the inter-session variability of the inversion results. The thickness of the top-most layer and the depth to the half-space top were specified to conform with the empirical λ-criterion. The initial estimates of V_S for each layer were obtained by mapping the respective experimental DCs into pseudo-values of V_S and discretising the resulting pseudo-V_S profiles to match the initially assumed layer structure (Xia, Miller, and Park 1999; Olafsdottir, Erlingsson, and Bessason 2020).

Figures 4*A–F* summarize the inversion results for the six DAQ sessions. The set of sampled V_S profiles whose associated theoretical DCs fall within one standard deviation of the target curve at all wavelengths are color-coded by misfit values. Hence, the profiles shown in yellow present the minimum-misfit solutions. The maximum investigated depth is, for each session, specified based on the $\lambda_{max}/2$ criterion using the respective composite DC. The minimum-misfit solutions for each session are compared in figure 4*G* and the corresponding time-averaged V_S profiles are shown in figure 4*H*. The variability of the inverted V_S and $V_{S,z}$ values is quantified using the COV-statistic in figure 4*I*, with COV_{V_S} and $COV_{V_{S,z}}$ defined as,

$$COV_{V_S}(z) = \frac{s}{\overline{V_S}} \quad (6)$$

$$COV_{V_{S,z}}(z) = \frac{s}{\overline{V_{S,z}}} \quad (7)$$

$\overline{V_S}$ and s (equation (6)) are the average and standard deviation of the interval V_S values at depth z. $\overline{V_{S,z}}$ (equation (7)) is the average of the $V_{S,z}$ values for a given z and s is the corresponding standard deviation.

The results in figure 4 show adequate agreement between the six independent measurements. The interval velocity profiles indicate a gradual increase in V_S with depth, ranging from 50–75

m/s for the surficial layer to around 320–430 m/s at 20–25 m depth. These values are consistent with investigations at comparable sites in the South Iceland Seismic Zone (SISZ) (Erlingsson, Olafsdottir, and Bessason 2022). The higher COV_{V_S} at shallow depth is attributed to the increased variability within the set of experimental DCs at short wavelengths (figs. 3*G* and 3*H*). These may further relate to subtle changes in groundwater level positions or surficial soil compaction between measurements. It should, however, be noted that the same limitations regarding sample size apply as for assessment of the inter-session COV_{V_R} (fig. 3*H*). Hence, the COV_{V_S} statistic and its average (fig. 4*I*) are only computed down to the depth of the shallowest interval V_S profile (i.e., 15.7 m for the M-13 session). Close to surface level, the variation of the estimated $V_{S,z}$ values follows the variation within the set of interval velocity profiles. However, it diminishes rapidly as the values of $V_{S,z}$ are computed over a larger depth interval, presenting an average $COV_{V_{S,z}}$ below 5 % as compared to an average COV_{V_S} around 10 %.

To further evaluate the reproducibility of the $V_{S,z}$ parameter, Table 2 gives the values of $V_{S,10}$, $V_{S,20}$ and $V_{S,30}$ as obtained using the population of accepted V_S profiles in the six-layer inversion (figs. 4*A–F*). For each session, the results are summarized by the mean $V_{S,z}$ value ($z \in \{10, 20, 30\}$ m) and coefficient of variation. The lowest and highest estimates of $V_{S,z}$ for each inversion are also given. In addition, Table 2 provides boundary estimates of $V_{S,10}$, $V_{S,20}$ and $V_{S,30}$ obtained for an expanded parameterization choice, i.e., inversions conducted in the same manner as described above but with the assumption of a four- to eight-layer soil model. The maximum and minimum values serve as a representation of the range in $V_{S,10}$, $V_{S,20}$ and $V_{S,30}$ estimates that may be expected from a single site investigation using a deterministic approach. For each session, the wider range of parameterizations expands the range of $V_{S,z}$ estimates as compared to the six-layer inversion. From an engineering design perspective, the observed differences are, however, relatively minor. The Arnarbæli site is characterized by thick sandy

sediments where a general increase in material stiffness with depth is expected. The $V_{S,30}$ estimates (equation (4)) are, therefore, likely somewhat biased towards lower values. Furthermore, as the estimated investigation depth varies between 15.7 and 26.5 m, the degree of underestimation is anticipated to differ between sessions, thus, making inter-session comparison of $V_{S,30}$ more uncertain than for $V_{S,10}$ and $V_{S,20}$.

Table 2 *$V_{S,10}$, $V_{S,20}$ and $V_{S,30}$ corresponding to the set of six-layered V_S profiles in figures 4A–F (6L) and boundary values obtained for an expanded set of parameterizations containing four to eight layers (4L–8L)*

		M-13		**M-14**		**M-15**		**M-17**		**M-18**		**M-19**	
		6L	**4L–8L**	**6L**	**4L–8L**	**6L**	**4L–8L**	**6L**	**4L–8L**	**6L**	**4L–8L**	**6L**	**4L–8L**
$\boldsymbol{V_{S,10}}$													
mean	[m/s]	129		142		131		128		133		142	
$COV_{V_{S,z}}$	[%]	2.06		2.00		1.93		2.06		2.67		1.53	
minimum	[m/s]	122	121	135	134	125	124	121	119	125	125	137	135
maximum	[m/s]	138	143	153	154	141	145	139	140	143	145	152	154
$\boldsymbol{V_{S,20}}$													
mean	[m/s]	177		194		184		179		181		196	
$COV_{V_{S,z}}$	[%]	2.00		2.55		2.80		2.25		2.31		2.00	
minimum	[m/s]	168	168	180	180	173	169	169	166	172	171	184	182
maximum	[m/s]	189	195	209	222	199	213	194	200	193	194	209	215
$\boldsymbol{V_{S,30}}$													
mean	[m/s]	203		229		224		213		211		233	
$COV_{V_{S,z}}$	[%]	2.41		2.08		2.23		2.65		1.58		1.60	
minimum	[m/s]	192	192	218	217	212	211	200	199	202	202	223	222
maximum	[m/s]	222	225	249	261	241	257	233	238	221	223	248	256

Comparison with Existing Measurements of V_S

To assess the performance of the processing and inversion tools, they were used to analyse a set of multi-channel time histories acquired at four benchmark sites in Southern and Central Norway, referred to as Onsøy, Halden, Øysand and Tiller-Flotten. The test site at Onsøy was established in the late 1960s by the Norwegian Geotechnical Institute (NGI) (Lunne, Long, and

Forsberg 2003) whilst the Halden, Øysand, and Tiller-Flotten research sites were developed in the Norwegian Geo-Test Sites (NGTS) project (L'Heureux et al. 2017). Table 3 summarizes their main characteristics and provides an overview of relevant previous work at each site.

Table 3 *Overview of site characteristics, MASW test parameters, and previous measurements of V_S at Onsøy, Halden, Øysand and Tiller-Flotten*

		Onsøy	**Halden**	**Øysand**	**Tiller-Flotten**
Site characteristics					
Characteristic soil type		Soft clay	Silt, clayey silt	Gravelly sand to silty sand	Quick clay
Unit weight		~16 kN/m^3	19–20.5 kN/m^3	18–19 kN/m^3	17–19 kN/m^3
Depth to bedrock		~40 m	~21 m in the southern part of the testing area	>80 m	>50 m
Detected groundwater table		Below the surficial crust	About 2–2.5 m below ground level	~2 m below ground level	~1–2 m below ground level
Existing measurements of shear wave velocity		SCPT, MASW, Lab	SCPT, SDMT, BE	SCPT, SDMT, MASW, BE	SCPT, SDMT, MASW
References		Lunne, Long, and Forsberg (2003), Long and Donohue (2007)	NGI (2018), Blaker et al. (2019)	Gundersen et al. (2018), Quinteros et al. (2019)	L'Heureux, Lindgård, and Emdal (2019)
Data acquisition					
No. geophones	[-]	24	24	24	24
Geophone spacing (source offsets)	[m]	1 (3–20) 2 (3–20)	1 (3–5)	2 (3–30)	1 (3–20) 2 (3–30)
No. records	[-]	78	35	30	99
Dispersion analysis					
DC frequency range	[Hz]	3.6–45.0	5.5–37.3	5.5–57.3	4.1–37.3
$\boldsymbol{COV_{V_R}}$ range	[%]	0.1–5.6	0.1–4.8	0.1–5.9	0.3–10.8

SCPT: Seismic Cone Penetration Test. SDMT: Seismic Dilatometer Marchetti Test. MASW: Multichannel Analysis of Surface Waves. Lab: Laboratory tests (unspecified). BE: Bender element test (laboratory).

Dispersion Data Processing and Inversion for Vs

The data acquisition at the four benchmark sites was conducted using the same equipment and by following the same field procedures as previously described. The test configurations are summarized in Table 3. An example of the subsequent data analysis is given in figure 5,

showing results from Øysand. The data acquisition and processing for Halden is described in Olafsdottir, Erlingsson, and Bessason (2020). At each test location, the receiver array(s) were placed as close as possible to relevant previous work at the site. A range of different source offsets was used with several shot repetitions for each array length-source offset combination to quantify the intra-session variability of the retrieved elementary DCs. The frequency range of the identified DCs is given in Table 3 along with the corresponding range in COV_{V_R}. Overall, the retrieved DC estimates show low variability, particularly for Halden, Onsøy and Øysand. A trend of increased COV_{V_R} at low frequencies, as shown for Øysand in figure $5B$, is further observed which is consistent with values obtained at other sites and reported in literature (e.g., Lai, Foti, and Rix 2005; Cox, Wood, and Teague 2014; Garofalo et al. 2016a; Roy and Jakka 2018; Passeri et al. 2021).

To mirror the common situation of limited (or no) a priori information on soil stratigraphy being available, the inversion of the composite DCs was conducted without using existing data to guide the model parameterization. Instead, a preliminary inversion was conducted using several different parameterizations consisting of two to nine layers (including the half-space). If two (or multiple) parameterizations produced a set of sampled V_S profiles whose forward response matched the experimental data equally well and showed comparable misfit values, the simpler model was chosen for further analysis. This preliminary analysis resulted in a four-layer model for Øysand and six layers for Onsøy, Halden, and Tiller-Flotten, respectively. The mass density profile for each site was defined using results of previous geotechnical investigations (Blaker et al. 2019; Lunne, Long, and Forsberg 2003; Gundersen et al. 2018; Quinteros et al. 2019; L'Heureux, Lindgård, and Emdal 2019). For the unsaturated surficial soil layer(s), the V_P values were, in each iteration, linked to the trial V_S profile through the Poisson's ratio. In lack of site-specific values, the Poisson's ratio was assessed using standard values for the particular soil types.

435 **Comparison with Invasive, Non-Invasive and Laboratory Measurements of Vs**

436 Figure 6 compares the MASW V_S profiles with independent assessments of V_S for the respective
437 sites. The MASW results are summarized by the minimum-misfit profile and the median of the
438 accepted interval V_S models, i.e., a profile comprised of the median of the $V_{S,1}$ values, the
439 median of the z_1 values, etc., as included in the set of accepted models ($V_{S,i}$ and z_i denote the
440 velocity of the i-th layer and the depth of the i-th layer interface, respectively).

441 Several SCPTs were carried out at Onsøy in 1984 and 2004 (Lunne, Long, and Forsberg 2003;
442 Bazin et al. 2016) and MASW measurements in 2005 (Long and Donohue 2007). The current
443 MASW results are consistent with the repeated SCPTs, particularly within the top 10–12 m
444 (fig. 6*A*). The 2005 MASW measurements indicate the same general velocity trend. Below 10–
445 12 m, the current results, however, show a slightly sharper increase in V_S than the existing data.
446 Results of laboratory measurements of V_S, conducted on block samples collected at 8–14 m
447 depth (Bazin et al. 2016), agree well with the in-situ measurements.

448 Figure 6*B* compares the inversion results for Halden with existing SCPT, SDMT, MASW and
449 bender element (BE) tests. The SDMT V_S profile is in good agreement with the current MASW
450 results. The SCPT profiles are slightly scattered. Nevertheless, the results of the current survey
451 are consistent with the general trend displayed by the SCPTs. The NGTS MASW
452 measurements were conducted along two arrays, HALM01 and HALM02 (Blaker et al. 2019).
453 Out of the two, HALM01 (fig. 6*B*, dashed grey line) was closer to the current array, whilst the
454 centre of HALM02 (unbroken grey line) was located approximately 50 m towards north-east.
455 The NGTS MASW results present significantly higher estimates of V_S than the other in-situ
456 tests, particularly down to around 4 m depth. However, Blaker et al. (2019) reported that the
457 inversion data fit for the two arrays was of limited quality, which may attribute to the observed
458 difference. The BE tests tend to indicate slightly lower V_S than was measured in-situ.

459 Various in-situ techniques have been used to characterize the gravelly-sandy-silty sediments at
460 Øysand, including SCPT, SDMT and MASW (NGTS data; Quinteros et al. 2019). There is
461 substantial scatter in the invasive data within the top 5 m. However, the current MASW results
462 are consistent with the general trend indicated by the SDMT and SCPTs (fig. 6*C*). They further
463 correspond well with the fairly constant V_S of approximately 200 m/s shown by the invasive
464 measurements at 5–16 m depth. Below that, the scatter in the invasive data increases again due
465 to site heterogeneities. The MASW survey resolution is substantially reduced in that depth
466 range, hence, the V_S profile is only shown for depths down to 16 m. The NGTS MASW surveys
467 are in good agreement with the current V_S profile. BE tests, conducted on samples collected at
468 the location of the in-situ measurements, further indicate comparable values of V_S as shown by
469 the current survey.

470 Figure 6*D* compares the results of the MASW survey at Tiller-Flotten to invasive and non-
471 invasive V_S profiles obtained for the site. The existing SCPT and SDMT results (L'Heureux,
472 Lindgård, and Emdal 2019) are consistent and indicate a gradual increase in V_S with depth. The
473 current interval V_S profiles present the same general trend, although they indicate a slightly
474 stiffer soil profile below around 12 m depth than the invasive measurements. However, the
475 spread in the SCPT data also increases below 12 m. A series of independent MASW
476 measurements (NGTS data) revealed comparable estimates of V_S as the current survey. The
477 resolution of the current measurements is, however, limited in the top-most 1.2–1.5 m due to
478 lack of high-frequency components in the experimental data. This makes direct comparison of
479 the respective MASW V_S profiles difficult for the surficial soils.

480

481 # Discussion

The dispersion data retrieved in the six DAQ sessions at Arnarbæli presented intra-session COV_{V_R} generally between 1.5 % and 5 %. Consistent with previous findings (e.g., Lai, Foti, and Rix 2005; Cox, Wood, and Teague 2014; Garofalo et al. 2016a; Roy and Jakka 2018; Passeri et al. 2021), its variation was found to depend on frequency, with the lower frequency components (<10 Hz) generally displaying the highest COV_{V_R}. DC estimates retrieved using different array configurations (within a given session) were in excellent agreement, further demonstrating the quality of the experimental data. However, its high-frequency content was not sufficient to identify experimental DCs above 30–45 Hz, thus, reducing the survey resolution at shallow depths (<1 m).

Inter-session comparison of the composite DCs indicated that the dispersion analysis is, overall, stable and provides consistent and repeatable results. The estimated inter-session variability (fig. 3*H*) tended to exceed the intra-session variability (figs. 3*A–F*). Nonetheless, the inter-session COV_{V_R} was typically around or below 5 %, which is consistent with intra-session values reported in literature (e.g., Passeri et al. 2021). Furthermore, as previously stated, the inter-session COV_{V_R} should be interpreted with caution due to the small sample size. The increased values at short wavelengths are primarily driven by the M-19 DC (fig. 3*G*) and that the number of retrieved DCs decreased rapidly at wavelengths shorter than 2.3 m (fig. 3*I*). Environmental factors, such as changes in groundwater level positions and surficial soil compaction between repeated measurements, may further contribute to the observed difference.

The respective DAQ sessions were conducted at different times of the year, spanning spring to fall. No systematic seasonal difference was observed. This is consistent with the findings of Beaty and Schmitt (2003), who conducted measurements from late spring to early fall at a site with small seasonal variations in groundwater level. Continuous measurements of the

506 groundwater table at Arnarbæli are not available and were therefore not modelled during the
507 inversion. Hence, correlating the short-wavelength dispersion data (or the inverted V_S profiles)
508 with potential changes in saturation of the surficial soils is not possible. However, the spring
509 and early summer of 2019 was very dry in South Iceland and the water level in the Ölfus River
510 by Arnarbæli was unusually low for that time of year (IMO data). It is therefore reasonable to
511 assume that the groundwater level was somewhat lower in the spring of 2019 than in an average
512 year, which may explain the deviation in the experimental M-19 DC at short wavelengths.

513 The variability within the set of minimum-misfit V_S profiles (COV_{V_S}, figs. 4*G* and 4*I*) was found
514 to be around two to three times the inter-session COV_{V_R}. The increased variability both relates
515 to the intra-session uncertainties of the experimental data, which are propagated to the
516 inversion, and interpretation ambiguities that inherently arise. These include the inversion non-
517 uniqueness and choice of layering parameterization. The observed range in COV_{V_S} (generally
518 between 5 % and 25 %) is, however, comparable to, or slightly lower than, reported values in
519 inter-analyst comparative studies that include a variety of data processing and inversion
520 techniques for the top 25 m of soil (Garofalo et al. 2016a). This was expected, as the repeated
521 measurements presented herein were all analysed by a single team using the presented
522 processing and inversion tools, thus including fewer sources of uncertainty. The set of
523 minimum-misfit profiles further yields estimates of $V_{S,z}$ (fig. 4*H*) which show comparable
524 variability ($COV_{V_{S,z}}$) as observed within the set of composite DCs. Hence, the effects of the
525 inversion non-uniqueness are reduced. These findings are in line with those observed in earlier
526 studies (e.g., Comina et al. 2011; Garofalo et al. 2016a; Roy and Jakka 2018).

527 The comparative analysis at the four benchmark sites indicated that the retrieved V_S profiles
528 were for all practical purposes very comparable to profiles obtained with invasive techniques,
529 thus verifying the performance of the analysis tools. At each site, the MASW arrays were

placed as close as possible to relevant previous investigations. However, some differences in the retrieved V_S values may be expected. The invasive tests are point measurements and thus only reflect the subsoil conditions directly at the point of penetration, whilst the MASW results average the soil properties over the area underlying the receiver array. This applies, particularly, to the Halden and Øysand sites, where previous studies have identified lateral variabilities in soil properties or stratigraphy. The retrieved V_S profiles further compared well with results of SWMs, conducted with different data acquisition and analysis tools, and results of available laboratory tests.

Conclusions

MASWavesPy is a Python package for processing and analysing active-source multi-channel surface wave registrations acquired using the linear data acquisition layout of MASW. The phase shift method is used to visualize the dispersion properties of Rayleigh waves and experimental DCs identified using a built-in GUI application. The package further provides a specific module to assess the spread in the experimental data and to combine experimental DCs retrieved from multiple surface wave registrations. The inversion module utilizes a Monte Carlo global-search, with the fast delta-matrix algorithm used for forward computations. Computationally intensive parts are written in Cython for improved code performance and computational speed. Hence, the new package provides highly improved computational time as compared to the original MATLAB MASWaves formulation. It further includes a set of additional tools and technical advancements to both the dispersion processing and inversion schemes, aimed at improving the efficiency and usability of the code. The MASWavesPy package is distributed as open-source software, allowing users to modify the code and adapt it

553 to individual use cases. It can be accessed through the Python Package Index (PyPI) at
554 https://pypi.org/project/maswavespy/, along with sample data.

555 For evaluation of the performance of the newly developed tool, MASW results were compared
556 with in-situ and laboratory measurements of V_S conducted by different teams of researchers at
557 four benchmark sites in Norway. It was shown that the V_S profiles obtained using
558 MASWavesPy were consistent with those obtained with a variety of other techniques. The
559 benchmark sites are considered as representative for normally dispersive silt, soft clay, silty
560 sand, and quick clay deposits, respectively. Hence, the results verify the performance of the
561 new package, and the algorithms therein, for use in civil engineering studies at sites
562 characterized by various commonly encountered types of soft soils. It is though worth noting
563 that none of the sites have a complex stratigraphic profile, such as strong velocity reversals,
564 stiff surficial layers, or bedrock at very shallow depth. Where such conditions are encountered,
565 other active-source data processing techniques, or the use of additional surface wave methods
566 supplementing MASW, may result in better performance and improved stiffness
567 characterization (e.g., Rahimi, Wood, and Teague 2021; Boaga et al. 2013; Olafsdottir,
568 Erlingsson, and Bessason 2023).

569 The present study set out to evaluate the inter-session variability of MASW measurements for
570 characterization of soft soil sites commonly encountered in engineering practise in many parts
571 of the world. For this purpose, measurements were conducted at a silty sand site in South
572 Iceland over a seven-year period and the variability of the analysis results assessed in terms of
573 Rayleigh wave phase velocity, interval V_S profiles, and $V_{S,z}$ for common reference depths. To
574 assess the repeatability of the analysis, the DAQ sessions were conducted by the same team, at
575 the same location, using the same measurement procedure and the same equipment. In brief,
576 the inter-session COV_{V_R} was typically found to be around or below 5 %, with the largest COV_{V_R}
577 being observed close to surface, possibly related to differences in environmental conditions

578 (i.e., surficial compaction and groundwater level positions). The average COV of the
579 population of minimum-misfit V_S profiles, as could be retrieved from repeated deterministic
580 studies, was found to be around two to three times the observed inter-session COV_{V_R}. Finally,
581 the set of minimum-misfit V_S profiles yielded estimates of $V_{S,z}$ with comparable values of
582 $COV_{V_{S,z}}$ as was observed for the set of composite DCs. Hence, the effects of the inversion non-
583 uniqueness are reduced. Although different modelling parameterizations can result in vastly
584 different estimates of the interval V_S profile, the results further indicate that the modelling
585 parameterization plays a lesser role when determining $V_{S,z}$ (given that the data fit for the
586 different parameterizations is comparable). In general, therefore, the results of this study
587 support earlier conclusions on the consistency and robustness of SWMs, including MASW, for
588 evaluation of $V_{S,z}$.

589 # Acknowledgements

590 This work was supported by the Icelandic Research Fund [grant numbers 206793-052 and
591 218149-051]; the University of Iceland Research Fund; the Icelandic Road and Coastal
592 Administration; and the Energy Research Fund of the National Power Company of Iceland.

593 The authors would like to thank the organizers of the NGTS project (www.geotestsite.no) for
594 assistance prior to and during the in-situ measurements at the Norwegian research sites, and
595 for providing access to results of geotechnical, geophysical and laboratory measurements
596 conducted at the sites. Finally, the authors would like to thank the anonymous reviewers for
597 their insightful comments and observations.

598

599 # References

600 Bazin, S., H. Anschütz, G. Sauvin, T. E. Helle, S. Gribben, S. Donohue, and M. Long. 2016.
601 "Geophysical characterisation of marine and quick clay sites: field and laboratory tests." In
602 *Proceedings of the 5th International Conference on Geotechnical and Geophysical Site*
603 *Characterisation*, edited by B. M. Lehane, H. E. Acosta-Martínez, and R. Kelly, vol. 2, 831–
604 836. Sydney, Australia: Australian Geomechanics Society.

605 Beaty, K. S., and D. R. Schmitt. 2003. "Repeatability of multimode Rayleigh-wave dispersion
606 studies." *Geophysics* 68, no. 3 (May/June): 782–790. https://doi.org/10.1190/1.1581031

607 Behnel, S., R. Bradshaw, C. Citro, L. Dalcin, D. S. Seljebotn, and K. Smith. 2010. "Cython:
608 The best of both worlds." *Computing in Science & Engineering* 13, no. 2 (March/April): 31–
609 39. https://doi.org/10.1109/MCSE.2010.118

610 Bessason, B., and S. Erlingsson. 2011. „Shear wave velocity in surface sediments." *Jökull*
611 61:51–64.

612 Beyreuther, M., R. Barsch, L. Krischer, T. Megies, Y. Behr, and J. Wassermann. 2010. "ObsPy:
613 A Python Toolbox for Seismology." *Seismological Research Letters* 81, no. 3 (May/June):
614 530–533. https://doi.org/10.1785/gssrl.81.3.530

615 Blaker, Ø., R. Carroll, P. Paniagua, D. J. DeGroot, and J.-S. L'Heureux. 2019. "Halden research
616 site: geotechnical characterization of a post glacial silt." *AIMS Geosciences* 5, no. 2: 184–234.
617 https://doi.org/10.3934/geosci.2019.2.184

618 Boaga, J., G. Cassiani, C. L. Strobbia, and G. Vignoli. 2013. "Mode misidentification in
619 Rayleigh waves: Ellipticity as a cause and a cure." *Geophysics* 78 no. 4 (July/August): EN17-
620 EN28. https://doi.org/10.1190/geo2012-0194.1

621 Boore, D. M. 2004. "Estimating $\bar{V}_S(30)$ (or NEHRP site classes) from shallow velocity models
622 (depths < 30 m)." *Bulletin of the Seismological Society of America* 94, no. 2 (April): 591–597.
623 https://doi.org/10.1785/0120030105

624 Boore, D. M., and M. W. Asten. 2008. "Comparisons of shear-wave slowness in the Santa
625 Clara Valley, California, using blind interpretations of data from invasive and noninvasive
626 methods." *Bulletin of the Seismological Society of America* 98, no. 4 (August): 1983–2003.
627 https://doi.org/10.1785/0120070277

628 BSSC. 2020. *NEHRP (National Earthquake Hazards Reduction Program) Recommended*
629 *Seismic Provisions for New Buildings and Other Structures (FEMA P-2082-1) 2020 Edition.*
630 *Volume 1. Part 1: Provisions and Part 2: Commentary*. Washington, DC: Building Seismic
631 Safety Council (BSSC).

632 Buchen, P. W., and R. Ben-Hador. 1996. "Free-mode surface-wave computations."
633 *Geophysical Journal International* 124, no. 3 (March): 869–887.
634 https://doi.org/10.1111/j.1365-246X.1996.tb05642.x

635 CEN. 2004. *EN1998-1:2004. Eurocode 8: Design of structures for earthquake resistance. Part*
636 *1: General rules, seismic actions and rules for buildings*. Brussels, Belgium: European
637 Committee for Standardization (CEN).

638 Comina, C., S. Foti, D. Boiero, and L. V. Socco. 2011. "Reliability of $V_{S,30}$ evaluation from
639 surface-wave tests." *Journal of Geotechnical and Geoenvironmental Engineering* 137, no. 6
640 (June): 579–586. https://doi.org/10.1061/(ASCE)GT.1943-5606.0000452

641 Cox, B. R., and D. P. Teague. 2016. "Layering ratios: a systematic approach to the inversion
642 of surface wave data in the absence of a priori information." *Geophysical Journal*
643 *International* 207, no. 1 (October): 422–438. https://doi.org/10.1093/gji/ggw282

644 Cox, B. R., and C. M. Wood. 2011. "Surface Wave Benchmarking Exercise: Methodologies,
645 Results, and Uncertainties." In *Geo-Risk 2011: Risk Assessment and Management*, edited by
646 C. H. Juang, K. K. Phoon, A. J. Puppala, R. A. Green, and G. A. Fenton, 845–852. Reston,
647 VA: American Society of Civil Engineers. https://doi.org/10.1061/41183(418)89

648 Cox, B. R., C. M. Wood, and D. P. Teague. 2014. "Synthesis of the UTexas1 surface wave
649 dataset blind-analysis study: Inter-analyst dispersion and shear wave velocity uncertainty." In
650 *Geo-Congress 2014: Geo-characterization and Modeling for Sustainability*, edited by M.
651 Abu-Farsakh, X. Yu, and L. R. Hoyos, 850–859. Reston, VA: American Society of Civil
652 Engineers. https://doi.org/10.1061/9780784413272.083

653 Donohue, S., and M. Long. 2008. "Assessment of an MASW approach incorporating discrete
654 particle modeling." *Journal of Environmental and Engineering Geophysics* 13, no. 2 (June):
655 57–68. https://doi.org/10.2113/JEEG13.2.57

656 Douglas, J., and B. Edwards. 2016. "Recent and future developments in earthquake ground
657 motion estimation." *Earth-Science Reviews* 160 (September): 203–219.
658 https://doi.org/10.1016/j.earscirev.2016.07.005

659 Endrun, B., M. Ohrnberger, and A. Savvaidis. 2010. “On the repeatability and consistency of
660 three-component ambient vibration array measurements.” *Bulletin of Earthquake Engineering*
661 8, no. 3 (June): 535–570. https://doi.org/10.1007/s10518-009-9159-9

662 Erlingsson, S., E. A. Olafsdottir, and B. Bessason. 2022. “Soil site stiffness categorization
663 based on MASW field testing.” In *Proceedings of the 20th International Conference on Soil*
664 *Mechanics and Geotechnical Engineering*, edited by M. M. Rahman, and M. Jaksa, 371–376.
665 Sydney, Australia: Australian Geomechanics Society.

666 Foti, S., F. Hollender, F. Garofalo, D. Albarello, M. Asten, P.-Y. Bard, C. Comina, C. Cornou,
667 B. Cox, G. Di Giulio, T. Forbriger, K. Hayashi, E. Lunedei, A. Martin, D. Mercerat, M.
668 Ohrnberger, V. Poggi, F. Renalier, D. Sicilia, and V. Socco. 2018. “Guidelines for the good
669 practice of surface wave analysis: a product of the InterPACIFIC project.” *Bulletin of*
670 *Earthquake Engineering* 16, no. 6 (June): 2367–2420. https://doi.org/10.1007/s10518-017-
671 0206-7

672 Gabriels, P., R. Snieder, and G. Nolet. 1987. “In situ measurements of shear-wave velocity in
673 sediments with higher-mode Rayleigh waves.” *Geophysical Prospecting* 35, no. 2 (February):
674 187–196. https://doi.org/10.1111/j.1365-2478.1987.tb00812.x

675 Garofalo, F., S. Foti, F. Hollender, P.-Y. Bard, C. Cornou, B. R. Cox, M. Ohrnberger, D. Sicilia,
676 M. Asten, G. Di Giulio, T. Forbriger, B. Guillier, K. Hayashi, A. Martin, S. Matsushima, D.
677 Mercerat, V. Poggi, and H. Yamanaka. 2016a. “InterPACIFIC project: Comparison of
678 invasive and non-invasive methods for seismic site characterization. Part I: Intra-comparison
679 of surface wave methods.” *Soil Dynamics and Earthquake Engineering* 82 (March): 222–240.
680 https://doi.org/10.1016/j.soildyn.2015.12.010

681 Garofalo, F., S. Foti, F. Hollender, P.-Y. Bard, C. Cornou, B. R. Cox, A. Dechamp, M.
682 Ohrnberger, V. Perron, D. Sicilia, D. Teague, and C. Vergniault. 2016b. “InterPACIFIC

683 project: Comparison of invasive and non-invasive methods for seismic site characterization.
684 Part II: Inter-comparison between surface-wave and borehole methods." *Soil Dynamics and*
685 *Earthquake Engineering* 82 (March): 241–254. https://doi.org/10.1016/j.soildyn.2015.12.009

686 Green, R. A., B. Halldorsson, A. Kurtulus, H. Steinarsson, and O. Erlendsson. 2012. "A unique
687 liquefaction case study from the 29 May 2008, M_w6.3 Olfus earthquake, Southwest Iceland."
688 In *Proceedings of the 15th World Conference on Earthquake Engineering*, vol. 31, 24736–
689 24745. Lisbon, Portugal: Sociedade Portuguesa de Engenharia Sismica (SPES).

690 Gundersen, A. S., S. Quinteros, J.-S. L'Heureux, and T. Lunne. 2018. "Soil classification of
691 NGTS sand site (Øysand, Norway) based on CPTU, DMT and laboratory results." In *Cone*
692 *Penetration Testing 2018*, edited by M. A. Hicks, F. Pisanò, and J. Peuchen, 323–328. Leiden,
693 The Netherlands: CRC Press/Balkema.

694 Halldórsson, B., and R. Sigbjörnsson. 2009. "The M_w6.3 Ölfus earthquake at 15:45 UTC on
695 29 May 2008 in South Iceland: ICEARRAY strong-motion recordings." *Soil Dynamics and*
696 *Earthquake Engineering* 29, no. 6 (June): 1073–1083.
697 https://doi.org/10.1016/j.soildyn.2008.12.006

698 Jónasson, K., B. Bessason, Á. Helgadóttir, P. Einarsson, G. B. Guðmundsson, B. Brandsdóttir,
699 K. S. Vogfjörd, and K. Jónsdóttir. 2021. "A harmonised instrumental earthquake catalogue
700 for Iceland and the northern Mid-Atlantic Ridge." *Natural Hazards and Earth System*
701 *Sciences* 21, no. 7 (July): 2197–2214. https://doi.org/10.5194/nhess-21-2197-2021

702 Kaynia, A. M. 2021. "Analysis and characteristics of dynamic response of large pile groups."
703 In *Analysis of Pile Foundations Subject to Static and Dynamic Loading*, edited by A. M.
704 Kaynia, 333–349. London: CRC Press.

705 Krischer, L., T. Megies, R. Barsch, M. Beyreuther, T. Lecocq, C. Caudron, and J. Wassermann.
706 2015. "ObsPy: a bridge for seismology into the scientific Python ecosystem." *Computational*

Science & Discovery 8, no. 1 (January): 014003. https://doi.org/10.1088/1749-4699/8/1/014003

Lai, C. G., S. Foti, and G. J. Rix. 2005. "Propagation of data uncertainty in surface wave inversion." *Journal of Environmental and Engineering Geophysics* 10, no. 2 (June): 219–228. https://doi.org/10.2113/JEEG10.2.219

L'Heureux, J.-S., T. Lunne, S. Lacasse, R. Carroll, S. O. Strandvik, Z. Ozkul, A. Instanes, A. Sinitsyn, S. Degago, and S. Nordal. 2017. "Norway's National GeoTest Site Research Infrastructure (NGTS)." In *Proceedings of the 19th International Conference on Soil Mechanics and Geotechnical Engineering*, edited by W. Lee, J. Lee, H.-K. Kim, and D.-S. Kim, 611–614. Seoul: Korean Geotechnical Society.

L'Heureux, J.-S., A. Lindgård, and A. Emdal. 2019. "The Tiller-Flotten research site: Geotechnical characterization of a very sensitive clay deposit." *AIMS Geosciences* 5, no. 4: 831–867. https://doi.org/10.3934/geosci.2019.4.831

Li, J., and B. Rosenblad. 2011. "Experimental study of near-field effects in multichannel array-based surface wave velocity measurements." *Near Surface Geophysics* 9, no. 4 (August): 357–366. https://doi.org/10.3997/1873-0604.2011012

Long, M. and S. Donohue. 2007. "In situ shear wave velocity from multichannel analysis of surface waves (MASW) tests at eight Norwegian research sites." *Canadian Geotechnical Journal* 44, no. 5 (May): 533–544. https://doi.org/10.1139/t07-013

Lunne, T., M. Long, and C. F. Forsberg. 2003. "Characterisation and engineering properties of Onsøy clay." In *Characterisation and Engineering Properties of Natural Soils*, edited by T. S. Tan, K. K. Phoon, D. W. Hight, and S. Leroueil, vol. 1, 395–428. A.A. Balkema: Lisse, The Netherlands.

NGI. 2018. *Field and laboratory test results Halden. Norwegian GeoTest Sites (NGTS). Factual report 20160154-04-R*. Oslo, Norway: Norwegian Geotechnical Institute (NGI).

Olafsdottir, E. A. "Multichannel Analysis of Surface Waves for Soil Site Characterization." PhD diss., University of Iceland, 2019.

Olafsdottir, E. A., S. Erlingsson, and B. Bessason. 2018a. "Tool for analysis of multichannel analysis of surface waves (MASW) field data and evaluation of shear wave velocity profiles of soils." *Canadian Geotechnical Journal* 55, no. 2 (February): 217–233. https://doi.org/10.1139/cgj-2016-0302

Olafsdottir, E. A., B. Bessason, and S. Erlingsson. 2018b. "Combination of dispersion curves from MASW measurements." *Soil Dynamics and Earthquake Engineering* 113 (October): 473–487. https://doi.org/10.1016/j.soildyn.2018.05.025

Olafsdottir, E. A., B. Bessason, S. Erlingsson, J.-S. L'Heureux, and S. Bazin. 2019. "Benchmarking of an open-source MASW software using data from three Norwegian GeoTest Sites." In *Proceedings of the 17th European Conference on Soil Mechanics and Geotechnical Engineering*, edited by H. Sigursteinsson, S. Erlingsson, and B. Bessason. Reykjavik, Iceland: Icelandic Geotechnical Society. https://doi.org/10.32075/17ECSMGE-2019-0772

Olafsdottir, E. A., S. Erlingsson, and B. Bessason. 2020. "Open-Source MASW Inversion Tool Aimed at Shear Wave Velocity Profiling for Soil Site Explorations." *Geosciences* 10, no. 8 (August): 322. https://doi.org/10.3390/geosciences10080322

Olafsdottir, E. A., S. Erlingsson, and B. Bessason. 2023. "Hybrid non-invasive characterization of soil strata at sites with and without embedded lava-rock layers in the South Iceland Seismic Zone." *Bulletin of Engineering Geology and the Environment* 82, no. 4 (April): 146. https://doi.org/10.1007/s10064-023-03136-0

754 Park, C. B., R. D. Miller, and J. Xia. 1998. “Imaging dispersion curves of surface waves on
755 multi-channel record.” In *SEG Technical Program Expanded Abstracts 1998*, 1377–1380.
756 Tulsa, OK: Society of Exploration Geophysicists. https://doi.org/10.1190/1.1820161

757 Park, C. B., R. D. Miller, and J. Xia. 1999a. “Multichannel analysis of surface waves.”
758 *Geophysics* 64, no. 3 (May): 800–808. https://doi.org/10.1190/1.1444590

759 Park, C. B., R. D. Miller, and J. Xia. 1999b. “Multimodal analysis of high frequency surface
760 wave.” In *SAGEEP ’99: Proceedings of the Symposium on the Application of Geophysics to*
761 *Engineering and Environmental Problems*, 115–122. Wheat Ridge, CO: Environmental and
762 Engineering Geophysical Society.

763 Passeri, F., C. Comina, S. Foti, and L. V. Socco. 2021. “The Polito Surface Wave flat-file
764 Database (PSWD): statistical properties of test results and some inter-method comparisons.”
765 *Bulletin of Earthquake Engineering* 19, no. 6 (April): 2343–2370.
766 https://doi.org/10.1007/s10518-021-01069-1

767 Quinteros, S., A. Gundersen, J.-S. L’Heureux, J. A. H. Carraro, and R. Jardine. 2019. “Øysand
768 research site: Geotechnical characterisation of deltaic sandy-silty soils.” *AIMS Geosciences*
769 5, no. 4: 750–783. https://doi.org/10.3934/geosci.2019.4.750

770 Rahimi, S., C. M. Wood, and A. K. Himel. 2022. “Practical guidelines for near-field mitigation
771 on array-based active surface wave testing.” *Geophysical Journal International* 229, no. 3
772 (June): 1531–1549. https://doi.org/10.1093/gji/ggac011

773 Rahimi, S., C. M. Wood, and D. P. Teague. 2021. “Performance of Different Transformation
774 Techniques for MASW Data Processing Considering Various Site Conditions, Near-Field
775 Effects, and Modal Separation.” *Surveys in Geophysics* 42, no. 5 (September): 1197–1225.
776 https://doi.org/10.1007/s10712-021-09657-1

Roy, N., and R. S. Jakka. 2018. “Effect of data uncertainty and inversion non-uniqueness of surface wave tests on $V_{S,30}$ estimation.” *Soil Dynamics and Earthquake Engineering* 113 (October): 87–100. https://doi.org/10.1016/j.soildyn.2018.02.030

Teague, D. P., C. M. Wood, and B. R. Cox. 2017. dpteague/PyMASWdisp. https://web.archive.org/web/20201028211745/https://github.com/dpteague/PyMASWdisp

Tran, K. T., and D. R. Hiltunen. 2011. “An assessment of surface wave techniques at the Texas A&M national geotechnical experimentation site.” In *Geo-Risk 2011: Geotechnical Risk Assessment and Management*, edited by C. H. Juang, K. K. Phoon, A. J. Puppala, R. A. Green, and G. A. Fenton, 859–866. Reston, VA: American Society of Civil Engineers. https://doi.org/10.1061/41183(418)91

Vantassel, J. 2021 jpvantassel/swprocess: latest (concept). Zenodo. https://doi.org/10.5281/zenodo.4584129

Vantassel, J. P., and B. R. Cox. 2021. “A procedure for developing uncertainty-consistent Vs profiles from inversion of surface wave dispersion data.” *Soil Dynamics and Earthquake Engineering* 145 (June): 106622. https://doi.org/10.1016/j.soildyn.2021.106622

Vantassel, J. P., and B. R. Cox. 2022. “SWprocess: a workflow for developing robust estimates of surface wave dispersion uncertainty.” *Journal of Seismology* 26: 731–756. https://doi.org/10.1007/s10950-021-10035-y

Vantassel, J. P., B. R. Cox, P. G. Hubbard, and M. Yust. 2022. “Extracting high-resolution, multi-mode surface wave dispersion data from distributed acoustic sensing measurements using the multichannel analysis of surface waves.” *Journal of Applied Geophysics* 205: 104776. https://doi.org/10.1016/j.jappgeo.2022.104776

799 Wathelet, M., D. Jongmans, and M. Ohrnberger. 2004. “Surface wave inversion using a direct
800 search algorithm and its application to ambient vibration measurements.” *Near Surface*
801 *Geophysics* 2, no. 4 (November): 211–221. https://doi.org/10.3997/1873-0604.2004018

802 Wathelet, M., J.-L. Chatelain, C. Cornou, G. Di Giulio, B. Guillier, M. Ohrnberger, and A.
803 Savvaidis. 2020 “Geopsy: A User-Friendly Open-Source Tool Set for Ambient Vibration
804 Processing.” *Seismological Research Letters* 91, no. 3 (May): 1878–1889.
805 https://doi.org/10.1785/0220190360

806 Wood, C. M., and B. R. Cox. 2012. “A comparison of MASW dispersion uncertainty and bias
807 for impact and harmonic sources.” In *Proceedings of GeoCongress 2012*, edited by R. D.
808 Hryciw, A. Athanasopoulos-Zekkos, and N. Yesillerd, 2756–2765. Reston, VA: American
809 Society of Civil Engineers. https://doi.org/10.1061/9780784412121.282

810 Xia, J., R. D. Miller, and C. B. Park. 1999. “Estimation of near-surface shear-wave velocity by
811 inversion of Rayleigh waves.” *Geophysics* 64, no. 3 (May): 691–700.
812 https://doi.org/10.1190/1.1444578

813 Yoon, S., and G. J. Rix. 2009. “Near-field effects on array-based surface wave methods with
814 active sources.” *Journal of Geotechnical and Geoenvironmental Engineering* 135, no. 3
815 (March): 399–406. https://doi.org/10.1061/(ASCE)1090-0241(2009)135:3(399)

816

Figures

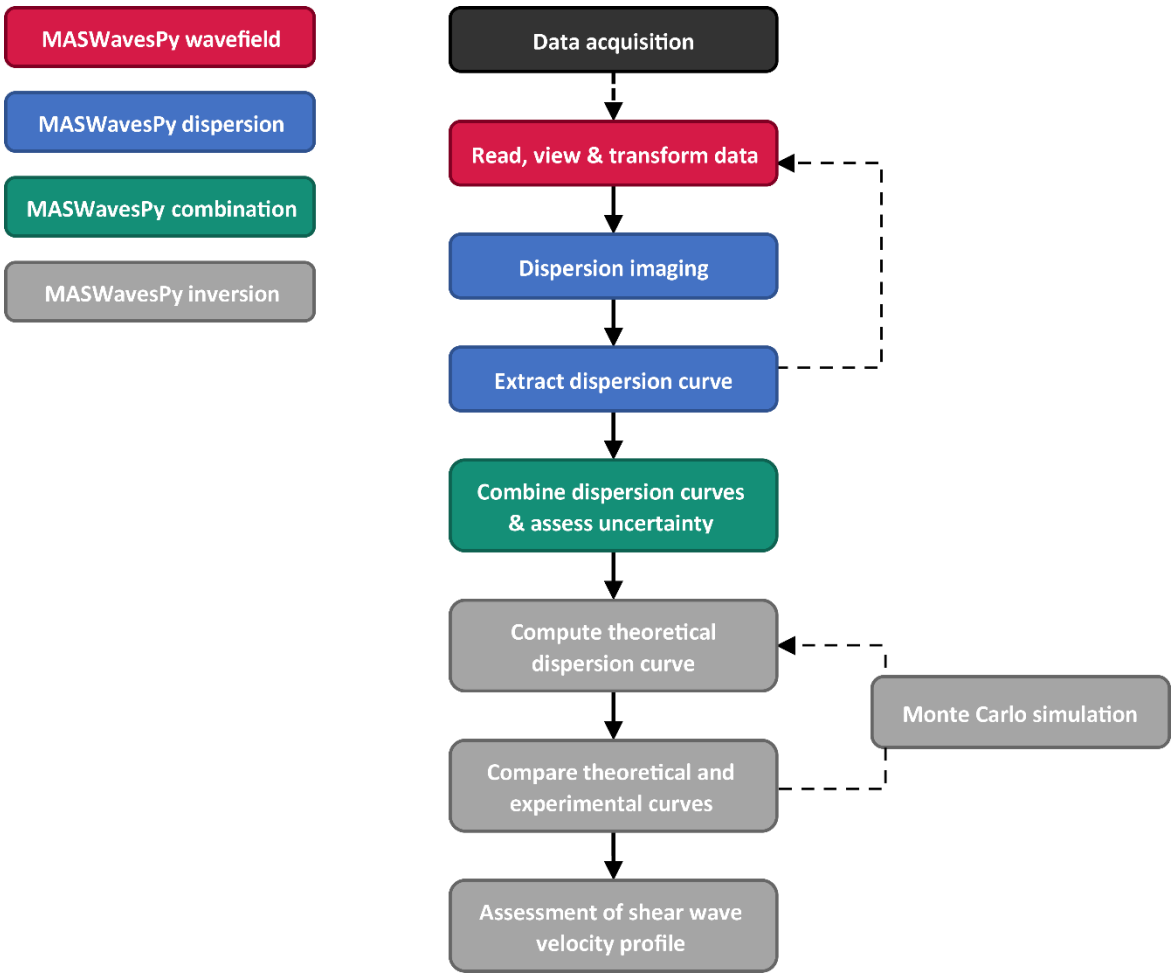

Fig. 1 *Workflow of MASWavesPy.*

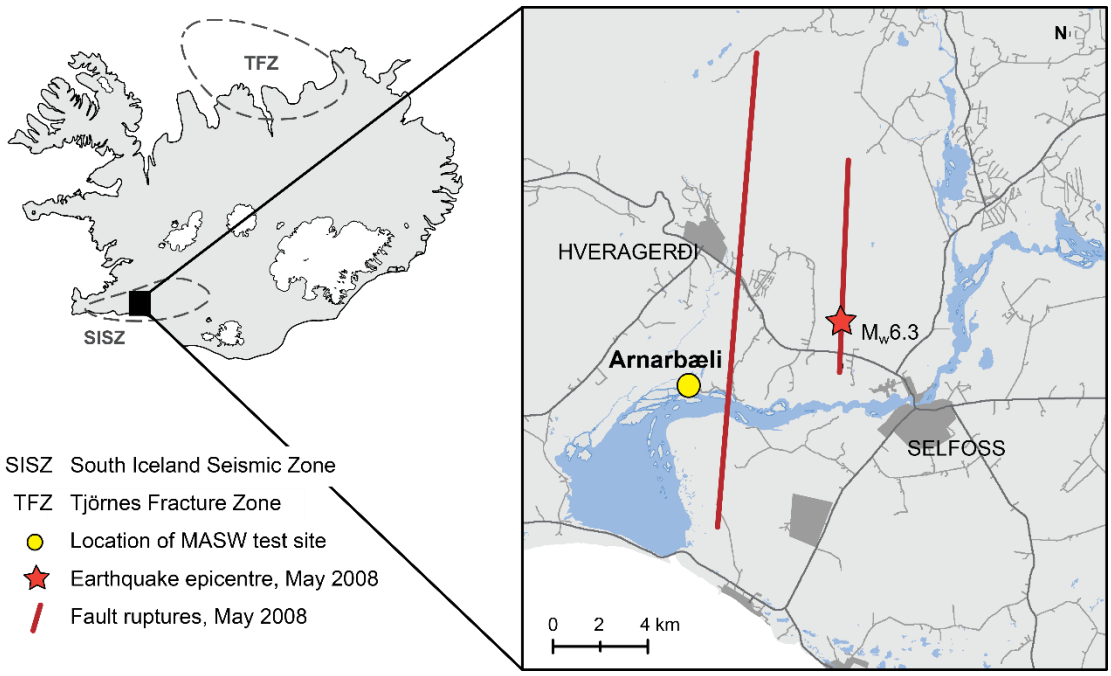

820

821 ***Fig. 2*** *Location of Arnarbæli test site on western bank of Ölfus River in South Iceland. The*
822 *map contains data from the IS 50V database of the National Land Survey of Iceland from*
823 *12/2020. Earthquake epicentre, ICEL-NMAR Earthquake Catalogue: Jónasson et al. (2021).*
824 *The two causative faults of the May 2008 Ölfus earthquake (Halldórsson and Sigbjörnsson*
825 *2009) are approximated by solid lines.*

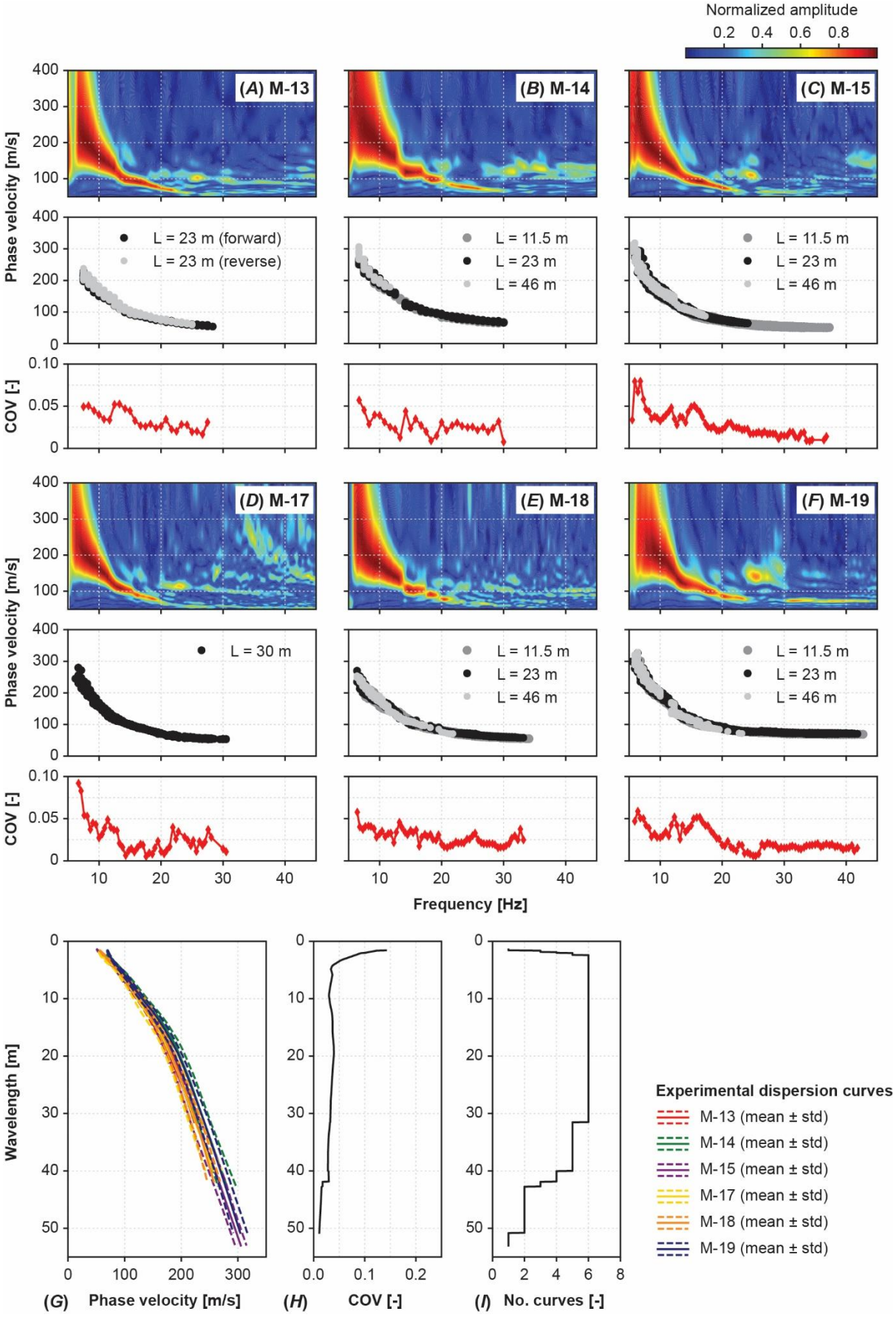
Normalized amplitude
0.2 0.4 0.6 0.8
(A) M-13
(B) M-14
(C) M-15
(D) M-17
(E) M-18
(F) M-19
Phase velocity [m/s]
COV [-]
L = 23 m (forward)
L = 23 m (reverse)
L = 11.5 m
L = 23 m
L = 46 m
L = 30 m
Frequency [Hz]
Wavelength [m]
(G) Phase velocity [m/s]
(H) COV [-]
(I) No. curves [-]
Experimental dispersion curves
M-13 (mean ± std)
M-14 (mean ± std)
M-15 (mean ± std)
M-17 (mean ± std)
M-18 (mean ± std)
M-19 (mean ± std)

826

827 ***Fig. 3 (A–F)*** *Top panels: Dispersion images acquired in field sessions M-13 through M-19 at*
828 *Arnarbæli. Middle panels: Elementary DCs obtained with receiver arrays of different lengths*
829 *or different shot positions. Bottom panels: Variation (COV) of extracted phase velocity values.*
830 ***(G–I)*** *Inter-session comparison. Composite mean DCs with standard deviation boundary*
831 *curves (**G**). Variability (COV) of the mean composite curves (**H**) and number of composite*
832 *curves obtained at a given wavelength (**I**).*

833

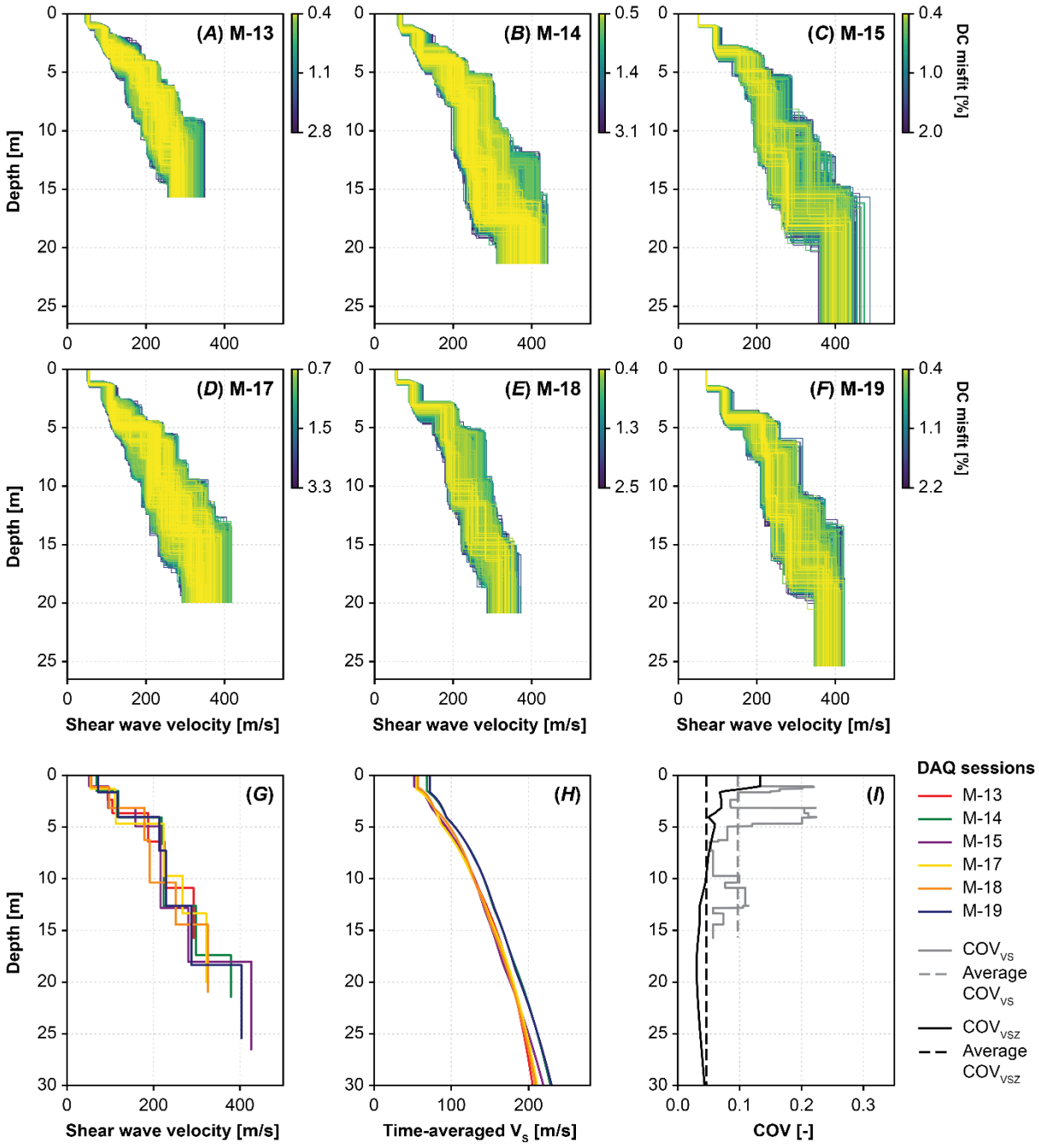

834

835 ***Fig. 4*** *V_S profiles whose associated theoretical DCs fall within one standard deviation of the*
836 *composite experimental curve for session* ***(A)*** *M-13,* ***(B)*** *M-14,* ***(C)*** *M-15,* ***(D)*** *M-17,* ***(E)*** *M-18,*
837 *and* ***(F)*** *M-19.* ***(G)*** *Comparison of the minimum-misfit V_S profiles and* ***(H)*** *the corresponding*
838 *$V_{S,z}$.* ***(I)*** *Variability (COV) of the minimum-misfit V_S and $V_{S,z}$ values with depth.*

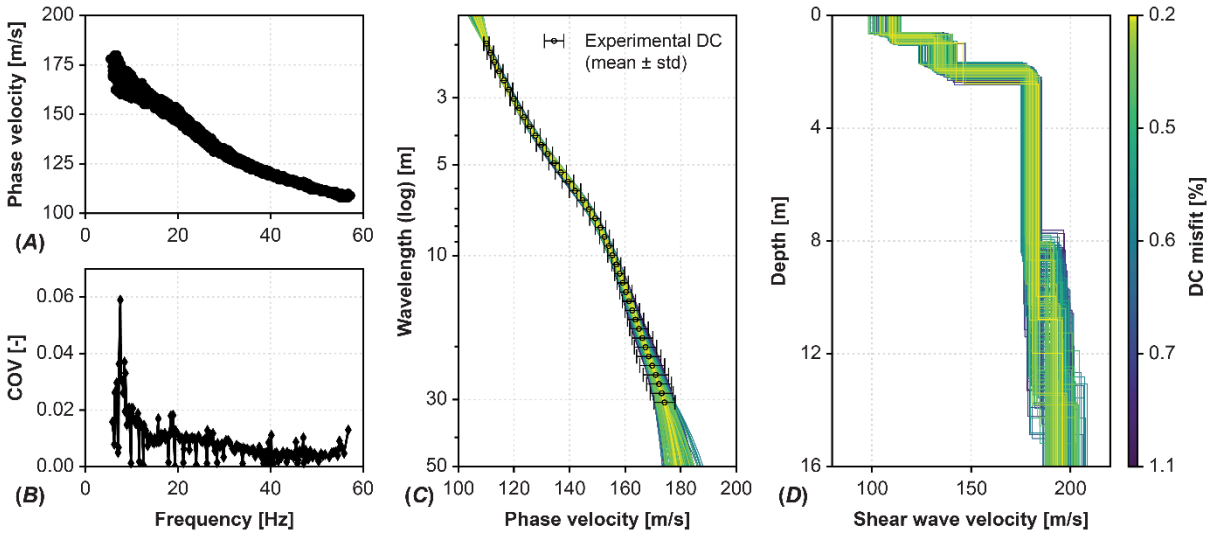

839

840 ***Fig. 5*** *MASW survey at Øysand.* ***(A)*** *Elementary dispersion curves.* ***(B)*** *Variation (COV) of the*

841 *extracted phase velocity values.* ***(C, D)*** *Sampled V_S profiles whose theoretical dispersion curves*

842 *fall within one standard deviation of the composite curve.*

843

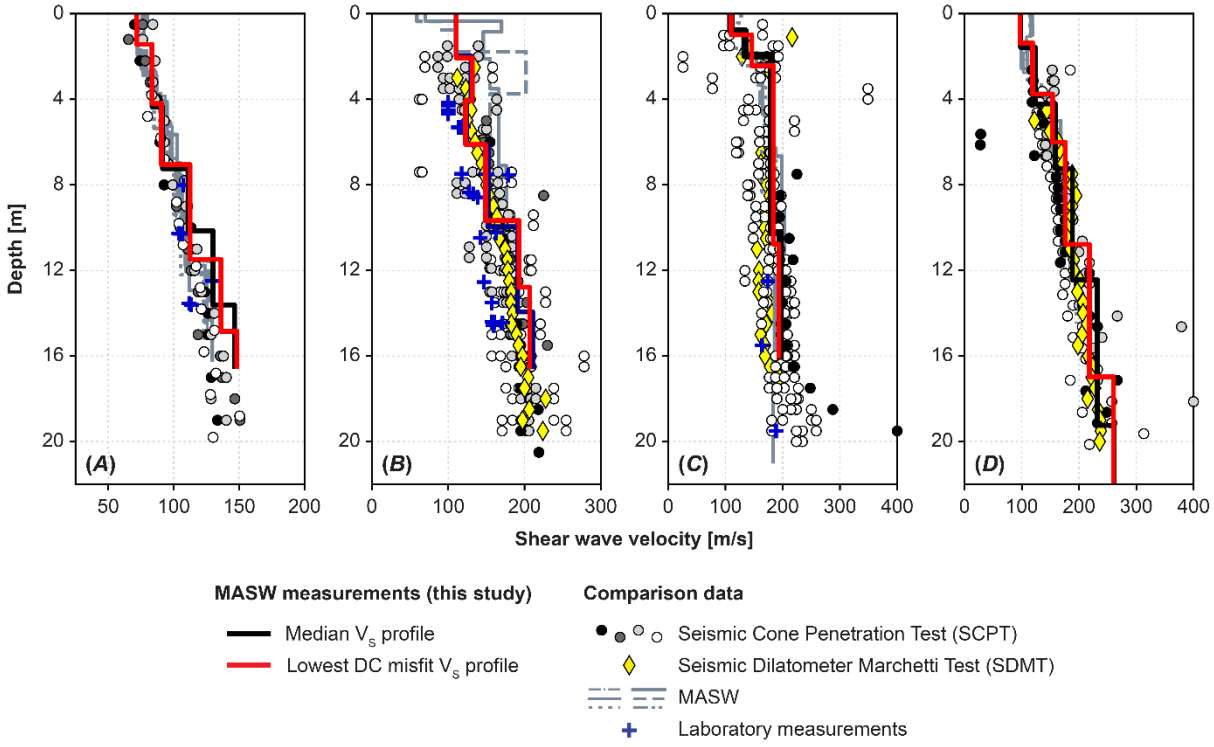

844

845 ***Fig. 6*** *Comparison of inverted V_S profiles and results of invasive, non-invasive and laboratory*
846 *measurements of V_S for* ***(A)*** *Onsøy,* ***(B)*** *Halden,* ***(C)*** *Øysand, and* ***(D)*** *Tiller-Flotten. SCPT,*
847 *SDMT, MASW and laboratory results from Long and Donohue (2007) [Onsøy], Bazin et al.*
848 *(2016) [Onsøy], NGI (2018) [Halden], Blaker et al. (2019) [Halden], Quinteros et al. (2019)*
849 *[Øysand], L'Heureux, Lindgård, and Emdal (2019) [Tiller-Flotten] and NGTS data [Øysand,*
850 *Tiller-Flotten].*

851